Journal of Molecular Structure, 214 (1989) 119–142
Elsevier Science Publishers B.V., Amsterdam — Printed in The Netherlands

VIBRATIONAL ANALYSIS OF CRYSTALLINE TRIGLYCINE*

T. SUNDIUS**, J. BANDEKAR and S. KRIMM

Biophysics Research Division and Department of Physics, University of Michigan, Ann Arbor, MI 48109 (U.S.A.)

(Received 31 January 1989)

ABSTRACT

We have refined vibrational force fields for polypeptides that permit excellent reproduction of the normal mode frequencies of such molecules. This is demonstrated in the present study, in which 80 IR and Raman bands of crystalline triglycine between 1800 and 200 cm^{-1} are reproduced with an average error of 6 cm^{-1}. A deuterated sample is shown by normal mode analysis to have remained protonated at the C-terminal peptide group. Such results show that normal mode analysis can now provide a rigorous base for spectral studies of conformation in peptides and proteins.

INTRODUCTION

Normal mode analyses of the vibrational spectra of small peptides of known structure are useful in validating force fields developed for polypeptides [1] and in providing convincing support for predictions of related unknown structures. As an example of this, our satisfactory analysis of the parallel-chain β structure in crystalline Val-Gly-Gly [2] enhances our confidence in the predictions of the vibrational spectrum of the general parallel-chain β-sheet [3]. Such studies also provide a rigorous base for using the observed spectra in further structural studies of these small peptides, and they help to analyze spectral details that need to be understood in order to permit the development of more complete force fields.

In this paper we present an analysis of the vibrational spectrum of a specific antiparallel-chain β-structure of crystalline triglycine, Gly_3 [4]. Previous structure studies on this molecule [5–8] have shown that it adopts at least two different crystal forms, probably corresponding to different molecular conformations. We have ascertained that our spectra are derived from the same kind of crystals on which the crystal structure analysis was done [4]. This avoids

*This paper is number 40 in a series on "Vibrational analysis of peptides, polypeptides, and proteins," of which ref. 3 is paper 39.

**Present address: Department of Physics, University of Helsinki, SF-00170 Helsinki, Finland.

0022-2860/89/$03.50

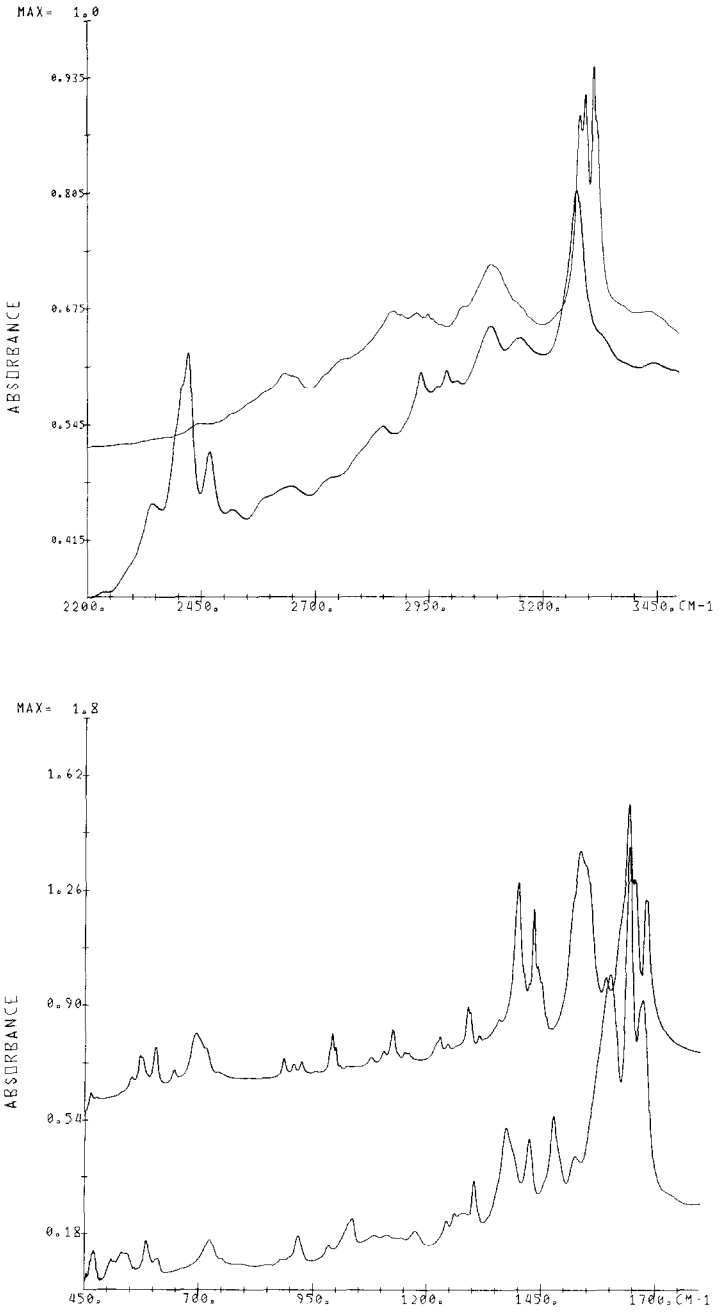

Fig. 1. IR spectra of triglycine (upper curve) and the deuterated derivative (lower curve).

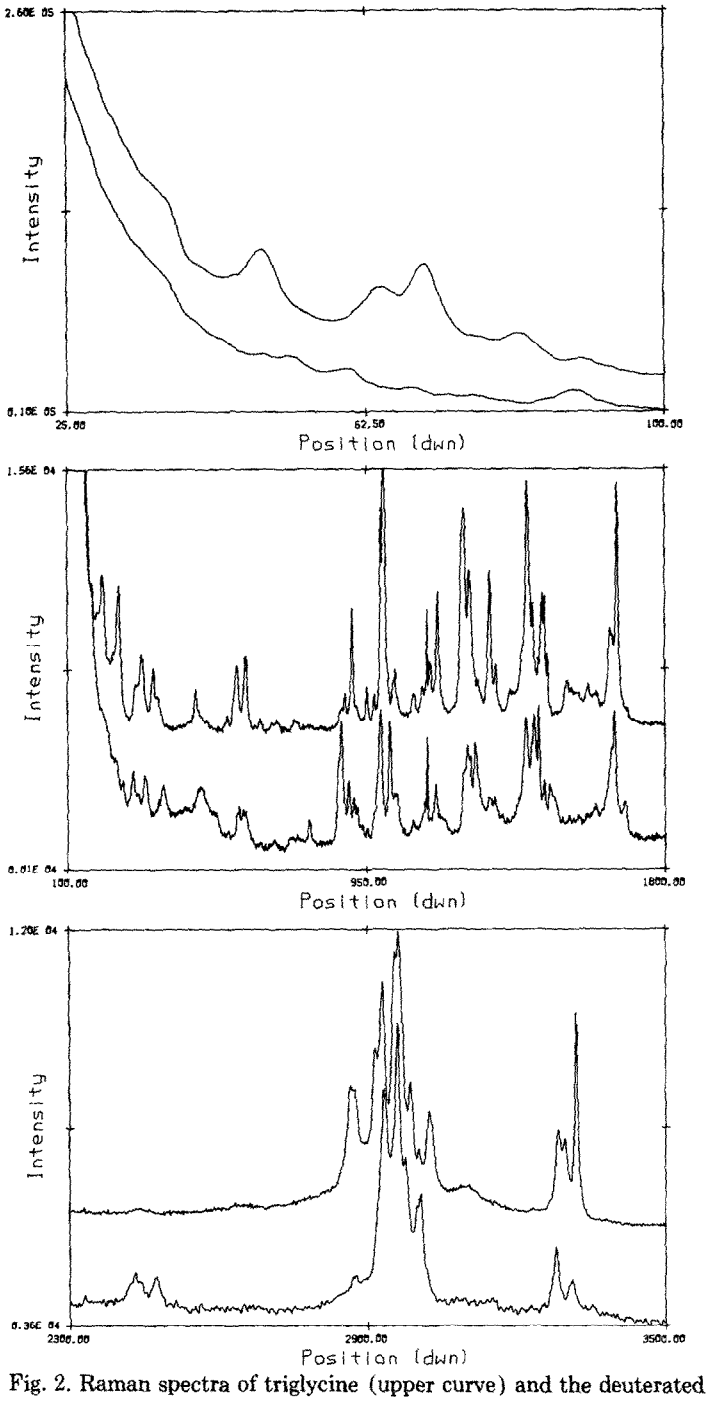

Fig. 2. Raman spectra of triglycine (upper curve) and the deuterated derivative (lower curve). (The intensity scale is for the protonated molecule. For the deuterated molecule, the intensity scales are: 0.4E05-3.2E05 (25-100 cm^{-1}), 4.2E03-1.2E04 (100-1800 cm^{-1}), and 0.1E03-4.2E04 (2300-3500 cm^{-1}).)

the complications of previous solid state IR studies [9], in which it was noted that different spectra were obtained from different forms, as well as of earlier solid state Raman studies [10], in which the sample was poorly defined.

Previous vibrational studies of Gly_3 have been based on a crude Urey–Bradley force field [11], and, for analysis of the conformation in aqueous solution [12], on a valence force field for diglycine. This analysis is based on our force field for polyglycine I [13], extending this to include force constants for the end groups by a refinement of the normal modes of crystalline diglycine. A preliminary report of the results has been presented [14].

EXPERIMENTAL

Triglycine was obtained as a powder sample from Sigma. Small crystals were grown from this material by slow evaporation of an aqueous methanol solution at room temperature. Tiny crystals were formed by rapid crystallization in vacuo. The spectra recorded from these three kinds of sample were significantly different, indicating differences in local molecular structure. The crystals formed by slow evaporation from methanol solution were found by X-ray diffraction [15] to correspond to those for which the crystal structure was determined [4], and these or tiny crystals grown on a watch-glass (which gave similar spectra) were used in our studies. Crystals of of N-deuterated Gly_3 were prepared in a similar manner, following three successive treatments with CH_3OD/D_2O followed by freeze-drying. (The freeze-drying procedure on normal samples gave our standard spectra.) As will be seen below, a specific pattern of deuteration resulted from this treatment.

Infrared spectra were obtained in KBr discs, at room and liquid nitrogen temperatures, using a Bomem DA3 FTIR spectrometer operating at a resolution of 2 cm^{-1}. Raman spectra were obtained from the crystals in a capillary tube, using a Spex 1403 spectrometer and 5145 Å excitation. The laser power was 500 mW, and a spectral band width of 2 cm^{-1} was used. Infrared spectra of Gly_3 and its deuterated derivative are given in Fig. 1, and Raman spectra are presented in Fig. 2.

NORMAL MODE CALCULATIONS

The unit cell of our form of Gly_3 is triclinic, space group $P\bar{1}$, with $a=11.656$ Å, $b=14.817$ Å, $c=4.823$ Å, $\alpha=88.45°$, $\beta=95.96°$, $\gamma=105.42°$, and $Z=4$, two molecules comprising the asymmetric unit (our labels A and B correspond to I and II [4], respectively). The unit cell is shown in Fig. 3, and the asymmetric unit is shown in Fig. 4. The conformations of the two molecules in this unit are very similar, except around the NH_3^+ groups, and they both have fully extended *trans*-planar structures (the C^α–C^α repeat distances are 7.27 Å (A) and 7.18 Å (B), compared to 7.044 Å in polyglycine I [16]). The backbone

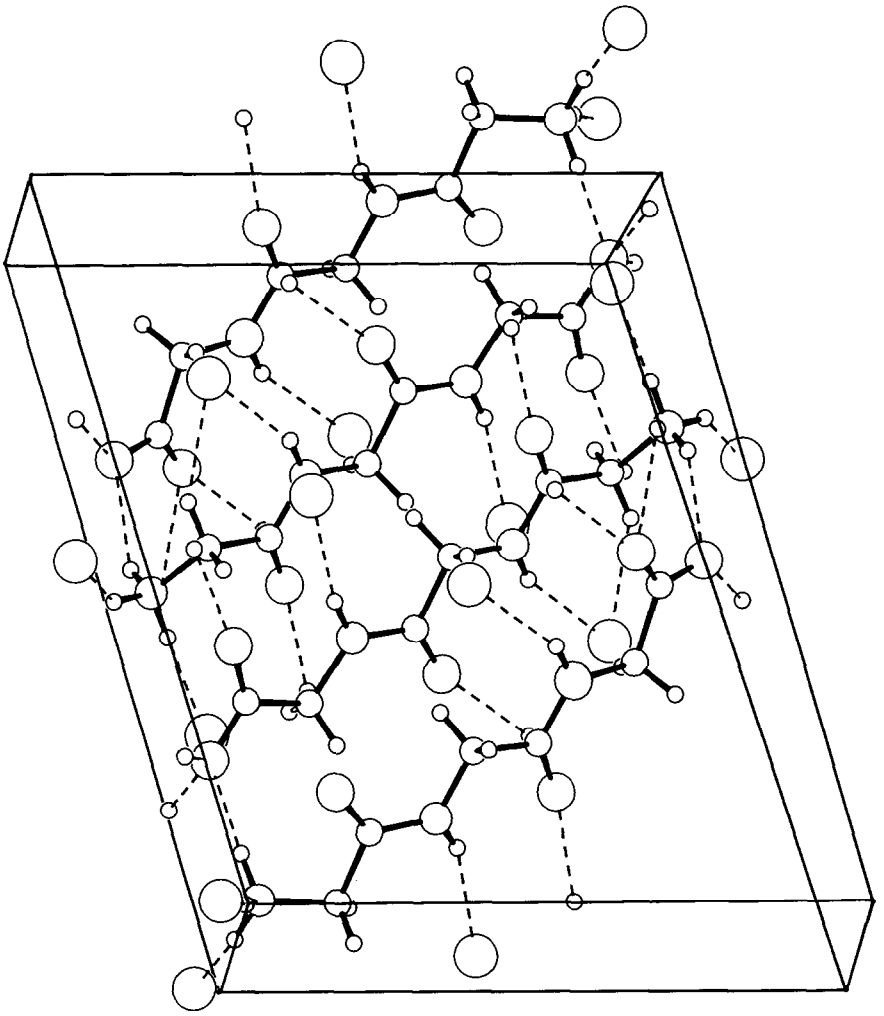

Fig. 3. Unit cell of triglycine (after ref. 4).

torsion angles are [4] A: $\psi_1 = -150°$, $\omega_1 = -176°$, $\phi_2 = 178°$, $\psi_2 = -172°$, $\omega_2 = -179°$, $\phi_3 = 173°$, and $\psi_3 = -173°$; B: $\psi_1 = -162°$, $\omega_1 = 176°$, $\phi_2 = -166°$, $\psi_2 = 175°$, $\omega_2 = -176°$, $\phi_3 = 173°$, and $\psi_3 = -169°$. The hydrogen-bonding pattern is quite complicated, involving bifurcated hydrogen bonds in some cases (see Table 6 of ref. 4). The peptide hydrogen bonds differ for the A and B molecules, with some being very weak ($d(\mathrm{H}\cdots\mathrm{O}) > 2.28$ Å, compared for example to $d(\mathrm{H}\cdots\mathrm{O}) = 1.75$ Å in polyglycine II and β-poly(L-alanine), 1.88 Å in α-poly(L-alanine), and 2.12 Å in polyglycine I [1]). The hydrogen bonds between end groups also differ for the A and B molecules. Table 1 presents the

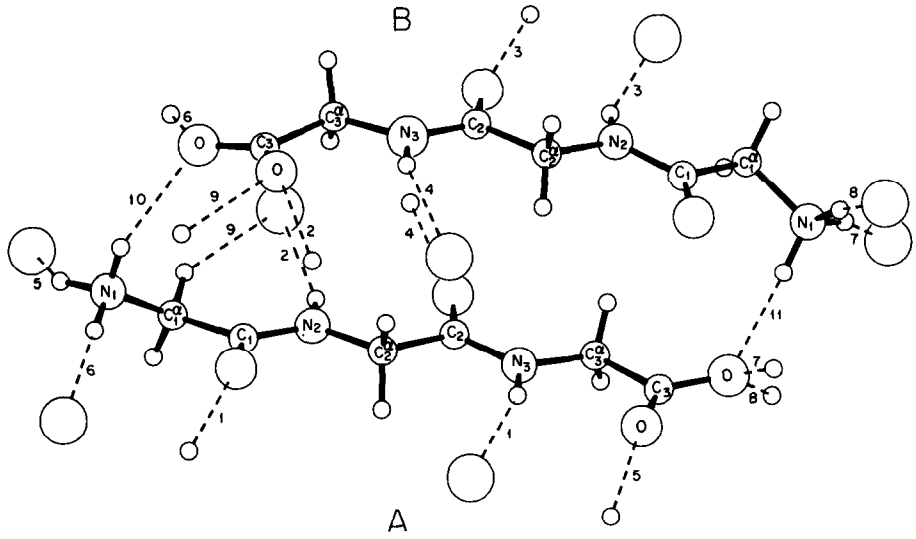

Fig. 4. Asymmetric unit of two molecules in unit cell of triglycine. Dotted lines show hydrogen bonds included in normal mode calculations (cf. Table 1).

TABLE 1

Hydrogen bond parameters and force constants used in normal mode calculations of Gly_3

Designation[a]	$d(H\cdot\cdot O)$[b]	$f(H\cdot\cdot O)$[c]
1	2.07	0.0755
2	2.12	0.0640
3	2.20	0.0450
4	2.28	0.0270
5	1.98	0.0960
6	1.86	0.1240
7	1.71	0.1509
8	1.77	0.1470
9[d]	2.34	0.0010
10	2.18	0.0500
11	1.99	0.0940

[a]See Fig. 4. [b]In Å. [c]In mdyn $Å^{-1}$. [d]$CH\cdot\cdot O$ bond; f set to 0.001.

hydrogen bonds that were included in the calculation (cf. Fig. 4), viz., intermolecular bonds with $d(H\cdots O) < 2.28$ Å, and the force constants associated with them.

In order to transfer our polyglycine I (PGI) force field [13] as a first approximation to Gly_3, we have used standard geometry for the peptide group [1]. The observed ϕ, ψ were used, and the actual hydrogen bond lengths were the basis for obtaining interpolated or extrapolated values of $f(H\cdots O)$, using PGI and PGII values from ref. 1. The geometric parameters of the end groups were the same as those used for Val-Gly-Gly [2], except that we took $d(N\text{-}H^+) = 1.04$ Å, in accordance with neutron diffraction results on diglycine [17,18]. The CO_2^- wagging coordinate was defined as previously [2].

The changes made in the main chain force constants from PGI were as follows. While we took $f(C_1{=}O)_A = f(C_2{=}O)_A = f(C_1{=}O)_B = f(C{=}O)_{PGI} = 9.882$, we set $f(C_2{=}O)_B = 9.750$, since this bond is 0.006 Å longer than the mean value of the other three C=O bonds (1.228 ± 0.001 Å). Since the $d(H\cdots O)$ vary significantly, we chose values of the $f(NH)$ to reflect the hydrogen-bond strength, using as a first approximation the $f(NH)$-$d(N\cdots O)$ relationship obtained from ab initio studies [19]. We took $f(C_2^{\alpha}H)$ equal to the PGI value of 4.564 but we set $f(C_3^{\alpha}H) = 4.820$, since this group next to CO_2^- gives rise to frequencies over 3000 cm^{-1} in diglycine, and we set $f(C_1^{\alpha}H) = 4.640$, to account for the relatively high (~ 2960 cm^{-1}) frequency for this group in diglycine (these changes required setting $f(C^{\alpha}H,C^{\alpha}H) = 0$, compared to its value of 0.01 in PGI, and adjusting $f(CC^{\alpha}H)$). The values of $f(C^{\alpha}NH)$ and $f(CNH)$ had to be adjusted slightly (from 0.527 to 0.487) to account for the amide II modes, probably a result of the difference in hydrogen bonding strengths between PGI and Gly_3. The amide V modes presented a bigger problem, undoubtedly related to the significantly different hydrogen bond strengths in the A and B molecules; we tried to compensate in part for this situation by keeping $f(NH\ ob)_B$ and $f(NH\ ob,CN\ t)_B$ at the PGI values and increasing the A counterparts to account for their stronger hydrogen bonds.

The main chain force constants are given in Table 2. The changes from PGI can only be considered approximations to the optimum modifications, since we have not undertaken a detailed force field refinement for the Gly_3 structure; the complexity in the hydrogen-bonding pattern is undoubtedly reflected in sensitive differences in force constants. At this stage, we chose only a minimal adjustment in a few force constants so that the most salient features of the spectra are reproduced. The broader problem of the detailed dependence of force field on hydrogen bonding and geometry will probably have to be dealt with through theoretical studies, such as our ab initio analysis of the glycine dipeptide [20]. The end group force constants are from our diglycine analysis, which was based on a refinement of initial values taken from a valence force field for the free molecule [21], and are also given in Table 2.

Infrared intensities and frequency shifts of some of the amide modes were calculated by dipole derivative coupling (DDC) [2], using dipole derivatives

TABLE 2

Adjusted peptide group and end-group force constants for Gly_3

Peptide group			End group					
			NH_3^+			CO_2^-		
Force constant[a]	Gly_3	PGI	Force const.[a]	Gly_3	PGI	Force const.[a]	Gly_3	PGI
$f(N_2H\ A)$	5.904	5.840	$f(NH)$	5.350	5.840	$f(C^\alpha C)$	4.409	4.409
$f(N_2H\ B)$	5.943	5.840	$f(NC^\alpha)_A$	4.500	5.043	$f(CO)$	9.500	9.882
$f(N_3H\ A)$	5.889	5.840	$f(NC^\alpha)_B$	4.700	5.043	$f(C^\alpha CO)$	1.109	1.246
$f(N_3H\ B)$	6.032	5.840	$f(HNH)$	0.590		$f(OCO)$	2.033	
$f(C_2{=}O)_B$	9.750	9.882	$f(HNC^\alpha)$	0.770		$f(CO\ ob)$	0.636	0.587
$f(C_1^\alpha H)$	4.640	4.564	$f(NC^\alpha H)$	0.715	0.715	$f(C^\alpha C\ t)$	0.294	0.037
$f(C_3^\alpha H)$	4.820	4.564	$f(NC^\alpha C)$	0.819	0.819	$f(C^\alpha C,CO)$	1.439	0.500
$f(C^\alpha H,C^\alpha H)_{1,3}$	0.000	0.010	$f(NC^\alpha\ t)$	0.200	0.037	$f(CO,CO)$	1.200	
$f(CC^\alpha H)$	0.715	0.684	$f(NC^\alpha,C^\alpha C)$	0.300	0.300	$f(C^\alpha C,OCO)$	0.519	0.450
$f(C^\alpha NH)$	0.487	0.527	$f(NC^\alpha,C^\alpha NH)$	0.144	0.294	$f(CO,C^\alpha CO)$	0.509	0.450
$f(CNH)$	0.487	0.527	$f(NC^\alpha,HNH)$	−0.150		$f(CO,C^\alpha CO')$	−0.509	
$f(NH\ ob)_A$	0.159	0.129	$f(NC^\alpha,NC^\alpha H)$	0.517	0.517	$f(CO,OCO)$	−0.135	
$f(NH\ ob,CN\ t)_A$	−0.1477	−0.1677	$f(NC^\alpha,CC^\alpha H)$	0.026	0.026	$f(CO\ ob,HC^\alpha C)$	−0.093	
			$f(NC^\alpha C,C^\alpha C)$	0.300	0.300	$f(CO\ ob,H^\alpha C^\alpha C)$	−0.093	
			$f(NC^\alpha C,NC^\alpha H)$	−0.031	−0.031	$f(CO\cdot\cdot H)$	0.050	
			$f(HNC^\alpha,NC^\alpha H)$	−0.012				
			$f(HNC^\alpha,NC^\alpha H^\alpha)$	0.012				
			$f(HNC^\alpha,HNC^\alpha)$	−0.040				

[a]Units: mdyn $Å^{-1}$ for stretch and stretch stretch constants; mdyn for stretch, bend constants; mdyn Å for all others.

for the peptide group obtained from ab initio studies of hydrogen-bonded *N*-methylacetamide [22].

RESULTS AND DISCUSSION

The observed and calculated frequencies of Gly_3 are given in Table 3, together with the potential energy distribution (PED) for each mode. For amide I, II and V modes, calculated IR intensities are given with the PEDs.

On examination of the spectra of the *N*-deuterated Gly_3, it became evident that the molecule was not completely deuterated; this is most clearly seen in the presence of an NH stretch mode at 3280 cm^{-1}, VS, in the IR. As we shall see, the evidence is strong that NH_3^+ is converted to ND_3^+ and that only one of the peptide nitrogens is deuterated. The results of normal mode calculations on both possible structures favor the $N_1D_3^+ N_2DN_3H$ structure (see discussion below). In Table 4, we present the calculated modes for this structure and our assignments of the observed bands. The reason for this pattern of deuteration is not apparent; it could be that the N_3 hydrogen is difficult to exchange, or, on the other hand, that it exchanges very readily and was subject to re-exchange on handling. In any event, this unusual pattern of deuteration has provided an interesting challenge to our predictive capabilities.

The NH stretch(s) modes, despite being perturbed by Fermi resonances [23], reveal a pattern that is undoubtedly related to the relative hydrogen-bond strengths, which would result in a frequency order of $\nu(N_{3A}H) < \nu(N_{2A}H) < \nu(N_{2B}H) < \nu(N_{3B}H)$. (This is not modified by taking Fermi resonance into account, using reasonable assignments of the ν_B values [23] in the, admittedly complex, ~3100 cm^{-1} region.) Four bands are observed, at 3284, 3298, 3315, and 3322 cm^{-1} in the IR, that can be assigned to these respective modes on the basis of relative f(NH) force constants determined from an ab initio f(NH)-d(N···O) relationship [19]. (We have matched the calculated with the observed 3284 cm^{-1} frequency and allowed the others to be determined by the f(NH)-d(N···O) relationship [19]; this is mainly for illustrative purposes, since we have not undertaken a Fermi resonance analysis of the 3100 cm^{-1} ν_B region). These assignments are further confirmed by the pattern resulting from deuteration: the highest and lowest frequency bands remain, the original bands shifting down to 3280 and 3313 cm^{-1}, while the two middle bands disappear, to be replaced by a pair of bands at 2424 and 2408 cm^{-1} (these two are well resolved and of reversed intensity ratio at liquid nitrogen temperature). The 2468 cm^{-1} band is probably amide B, its higher value than amide A being similar to the situation in poly(L-alanine-ND) [23]. The presence of bands near the values predicted for ND_3^+ (~2360–2200 cm^{-1}) supports our assertion that deuteration of this end group has occurred. Thus, the patterns of NH s and ND s modes are consistent with the deuterated molecule being $N_1D_3^+ N_2DN_3H$.

TABLE 3

Observed and calculated frequencies (in cm^{-1}) of Gly_3

Observed[a]		Calculated		Potential energy distribution[b]
Raman	IR	g	u	
3320MS	3322W	3313	3313	N_3H sB(99)
	3315VS	3295	3293	N_2H sB(99)
3297W	3298S	3286	3286	N_2H sA(99)
3285M	3284S	3283	3284	N_3H sA(99)
		3183	3177	H_3 as1B(66),H_3 as2B(31)
		3175	3175	H_3 as2B(67),H_3 as1B(31)
		3172	3170	H_3 as1A(72),H_3 as2A(26)
		3162	3161	H_3 as2A(72),H_3 as1A(26)
3101W	3102MW			amide B
3088VW	3088MW			amide B
		3075	3069	H_3 ssB(97)
		3056	3056	H_3 ssA(98)
3030sh	3030VVW	3010	3010	C_3H_2 asB(100)
3024M	3022VVW	3010	3010	C_3H_2 asA(100)
3002VVW				
2986W				
2962VS	2963VW	2957	2957	C_1H_2 asA(99)
2954S	2950W	2956	2956	C_1H_2 asB(99)
2930S		2936	2936	C_3H_2 ssB(99)
		2936	2936	C_3H_2 ssA(99)
	2925W	2928	2928	C_2H_2 asB(99)
2916sh		2927	2927	C_2H_2 asA(99)
2876M	2878W*	2881	2881	C_1H_2 ssB(99)
		2881	2881	C_1H_2 ssA(99)
2866M	2862W*	2861	2861	C_2H_2 ssB(99)
		2861	2861	C_2H_2 ssA(99)
	1685MS			
	1680MS		1686	C_2O sA(54),C_1O sA(19),C_2N sA(14) [14.7]
		1682		C_1O sB(66),C_1N sB(18),$C_1^{\alpha}CN$ dB(10)
1682sh		1679		C_2O sA(60),C_2N sA(16),C_1O sA(14)
1666VS		1663		C_2O sB(72),C_2N sB(20),$C_2^{\alpha}CN$ dB(11)
	1661sh		1661	C_1O sA(53),C_2O sA(20),C_1N sA(15) [4.7]
	1657W		1668	C_1O sB(72),C_1N sB(20),$C_1^{\alpha}CN$ dB(11) [9.0]
1645MW		1647		C_1O sA(54),C_1N sA(15),C_2O sA(13)
	1644VS		1648	C_2O sB(72),C_2N sB(20),$C_2^{\alpha}CN$ dB(11) [16.1]
	1630sh	1639	1639	H_3 ab2A(52),H_3 ab1A(32),H_3 r1A(12)
	1623sh	1618	1618	H_3 ab1B(83),H_3 r2B(10)
		1610	1610	H_3 ab2B(83),H_3 r1B(10)
		1608	1608	H_3 ab1A(57),H_3 ab2A(34)
1607W		1581	1581	O_2 asB(104)
1583W	1593W	1576	1576	O_2 asA(104)
		1574		N_2H ibB(21),H_3 sbB(13),$C_1^{\alpha}C$ sB(10),C_1N sB(9)
1554VW		1565		N_2H ibA(21),$C_1^{\alpha}C$ sA(12),C_1N sA(11),H_3 sbA(9)

TABLE 3 (continued)

Observed[a]		Calculated		Potential energy distribution[b]
Raman	IR	g	u	
			1551	N_2H ibA(22),$C_1^{\alpha}C$ sA(13),C_1N sA(11),H_3 sbA(10) [1.3]
	1553MS			H_3 sbB(17),N_3H ibB(17),C_2N sB(10),$C_2^{\alpha}C$ sB(9) [11.2]
			1550	
	1548VW*		1542	N_2H ibB(21),H_3 sbB(14),$C_1^{\alpha}C$ sB(11),C_1N sB(10) [0.4]
1535W		1538		H_3 sbB(20),N_3H ibB(18),C_2N sB(10),$C_2^{\alpha}C$ sB(10)
	1538S		1528	N_3H ibA(18),$C_2^{\alpha}C$ sA(11),C_2N sA(10),H_3 sbA(9) [8.8]
		1526		N_3H ibA(19),$C_2^{\alpha}C$ sA(11),H_3 sbA(11),C_2N sA(11)
1523W	1522sh	1515	1516	H_3 sbB(55),N_2H ibB(12)
		1505	1505	H_3 sbA(65),N_2H ibA(9)
		1466	1466	C_3H_2 bA(18),C_1H_2 bA(14),C_2H_2 wA(11)
1467W	1465sh			C_2H_2 bA(10),O_2 ssA(10)
		1466	1466	C_2H_2 bB(20),C_1H_2 bB(18),C_3H_2 bB(12)
1459M		1448	1449	C_1H_2 bB(39),C_3H_2 bB(24),O_2 ssB(10),N_2H ibB(5)
1452M	1453VW	1448	1448	C_1H_2 bA(37),C_3H_2 bA(23),O_2 ssA(12),N_2H ibA(6)
	1446W	1440	1440	C_2H_2 bB(63),C_3H_2 bB(14)
1440VW	1437MS	1435	1434	C_2H_2 bA(63),C_1H_2 bA(14)
1425W	1427VW	1415	1415	C_3H_2 bA(43),O_2 ssA(17),C_3H_2 wA(12),C_2H_2 bA(11)
	1416sh	1412	1412	C_3H_2 bB(41),C_3H_2 wB(19),O_2 ssB(11)
1410VS		1410	1409	O_2 ssA(31),C_2H_2 wA(17),$C_3^{\alpha}C$ sA(15), O_2 bA(13),C_2H_2 bA(12),N_3H ibA(7)
	1402S	1400	1400	O_2 ssB(34),C_2H_2 wB(19),O_2 bB(14), $C_3^{\alpha}C$ sB(13),N_3H ibB(7)
1377VW		1378	1378	C_3H_2 wA(37),C_1H_2 wA(10)
1369VW		1372	1373	C_3H_2 wB(32),C_1H_2 wB(18), $C_3^{\alpha}C$ sB(11),O_2 ssB(10)
1360W	1361W	1350	1350	C_1H_2 wA(49),C_2H_2 wA(12),N_2H ibA(5)
1332sh	1330VW	1349	1349	C_1H_2 wB(38),C_2H_2 wB(19),C_3H_2 wB(12)
1319W	1317W			
1303MS	1298W	1284	1284	C_2H_2 twA(48),C_1H_2 twA(22)
	1293M	1276	1276	C_1H_2 twB(54),N_2H ibB(7)
1277sh		1272	1272	C_1H_2 twA(50),C_2H_2 twA(39)
1269VW		1265	1265	C_3H_2 twB(32),C_2H_2 twB(32), N_3H ibB(6)
	1265VW	1261	1261	C_2H_2 twB(48),C_1H_2 twB(28)
		1259	1260	C_3H_2 twA(59),N_3H bA(6)
	1248W	1243	1243	N_2H ibB(24),C_3H_2 twB(15),NC_2^{α} sB(10)
1244M		1236	1237	N_2H ibA(26),C_3H_2 twA(14),H_3 r2A(7)
1228VS	1231MW	1227	1226	C_3H_2 twB(33),N_3H ibB(26),C_3H_2 wB(11)
1224W	1223VW	1218	1218	N_3H ibA(29),C_3H_2 twA(22),C_3H_2 wA(13)
	1218sh*	1207	1207	H_3 r2A(62),C_1H_2 rA(11)
1195sh		1192	1192	H_3 r2B(66),C_1H_2 rB(16),H_3 ab1B(5)
	1162W	1164	1164	H_3 r1B(66)
1153M	1153W	1155	1155	H_3 r1A(71),H_3 ab2A(8)
1132W	1127M	1140	1139	NC_2^{α} sB(28),NC_3^{α} sB(28)

TABLE 3 (continued)

Observed[a]		Calculated		Potential energy distribution[b]
Raman	IR	g	u	
1110W	1107W	1110	1110	NC_2^{α} sA(48),NC_3^{α} sA(17)
1085W	1080W	1085	1085	NC_3^{α} sB(37),NC_1^{α} sB(21),NC_2^{α} sB(16)
1043sh	1043VW	1040	1040	NC_3^{α} sA(45),NC_1^{α} sA(29)
1032W	1025VW	1021	1021	NC_1^{α} sB(60),NC_2^{α} sB(19)
1000VS	1001W	1001	1002	NC_1^{α} sA(45),NC_2^{α} sA(14),NC_3^{α} sA(11)
992M	994MS	994	993	C_2H_2 rB(77)
974W	972VW	977	976	C_2H_2 rA(27),$C_3^{\alpha}C$ sA(21)
		966	966	$C_3^{\alpha}C$ sB(34),O_2 bB(15)
	965W	965	965	C_2H_2 rA(51),$C_3^{\alpha}C$ sA(10)
952MW	950sh	946	945	$C_2^{\alpha}C$ sA(18)
		941	941	C_3H_2 rB(19),$C_2^{\alpha}C$ sB(13)
923W	926MW	937	937	C_3H_2 rA(75)
		935	934	C_3H_2 rB(66)
909M	911sh*	922	922	C_1H_2 rB(67),H_3 r2B(14)
	908MW	918	918	C_1H_2 rA(68),H_3 r2A(11)
890W	887M	904	905	$C_1^{\alpha}C$ sA(20)
		902	903	$C_1^{\alpha}C$ sB(17),C_1N sB(11)
878VW				
753VW	755sh*	759	758	O_2 bA(19)
746W	744W	744	744	O_2 bB(21),$C_2^{\alpha}C$ sB(10),C_2O ibB(10)
717VW	718W	718	720	C_2N tA(41),N_3H obA(17) [0.4]
703sh		697		C_1N tA(21),O_2 bA(16),C_2N tA(16), N_2H obA(14),$C_3^{\alpha}C$ sA(11),N_3H obA(6)
	706MS		690	C_1N tA(18),C_2N tA(16),O_2 bA(15), N_2H obA(13),$C_3^{\alpha}C$ sA(10),N_3H obA(6) [1.7]
683W	689sh*	688	688	O_2 bB(15),$C_3^{\alpha}C$ sB(13),C_1O ibB(12), $C_1^{\alpha}C$ sB(11)
695W	695S	672	680	C_1N tA(53),N_2H obA(20) [2.3]
648W	648MW	643	643	C_2O ibA(26),C_1O ibA(13),N_2H obA(5) [0.2]
		640	640	C_1O obB(29),C_2O ibB(15),C_2O obB(11)
634VW		632		C_1N tB(16),C_1O ibB(13),C_2O ibB(11),C_1O obB(10)
		630	630	O_2 wB(70)
		629	630	O_2 wA(82)
			628	C_1O ibB(15),C_1O obB(15),C_1N tB (14),C_2O ibB(10)
		613	613	C_2O obB(37),C_2N tB(16),C_1O obB(12)
606S	602sh*	612	612	C_2O obA(23),C_1O obA(20),C_2O obB(11), C_1O ibA(10)
609S	607S	600	609	C_2N tB(53),N_3H obB(41) [1.6]
	589sh*	592	590	C_2O obA(37),C_2N tB(22), N_3H obB(15),C_1O obA(10) [0.5]
582S	578M	580	581	O_2 rA(26),$C_2^{\alpha}CN$ dA(21)
572sh	573M	579	580	O_2 rB(23),$C_2^{\alpha}CN$ dB(21)
555W	555W	554	563	C_1N tB(99),N_2H obB(49) [1.5]
531VW	534sh			
496VW				

TABLE 3 (continued)

Observed[a]		Calculated		Potential energy distribution[b]
Raman	IR	g	u	
		467		O_2 rA(27),C_1^{α}CN dA(26)
466MW	466W		465	O_2 rB(29),C_1^{α}CN dB(23)
		465		O_2 rB(29),C_1^{α}CN dB(24)
			464	O_2 rA(27),C_1^{α}CN dA(25)
357W		382	381	NC_1^{α} tB(62)
344MW		359	360	NC_1^{α} tA(64)
		315	318	C_2^{α}CN dB(24),O_2 rB(14),C_1^{α}CN dB(11)
311MW		311	309	C_2^{α}CN dA(19),O_2 rA(11), C_1^{α}CN dA(10)
		299	298	N_3H obB(23),C_3^{α}C tB(18),N_2H obB(7)
295W		292	292	NC_1^{α}C dA(33),H··O s6(12),N_2H obA(8)
		280	280	NC_1^{α}C dB(13),C_3^{α}C tA(14),N_3H obB(7),N_3H obA(7)
		272	273	NC_1^{α}C dB(13),C_3^{α}C tA(11),N_3H obA(8)
			268	C_2O ibB(14),NC_3^{α}C dB(10),CNC_3^{α} dB(10), C_1O ibB(10),NC_1^{α}C dB(10)
		266		C_2O ibB(20),CNC_3^{α} dB(15),NC_3^{α}C dB(11), NC_2^{α}C dB(10)
246S		259	260	C_2O ibA(16),NC_3^{α}C dA(16), CNC_3^{α} dA(15),N_3H obA(11),NC_2^{α}C dA(10)
230sh		221	224	CNC_2^{α} dA(13), N_2H obA(11)
		216	218	N_2H obB(16), CNC_3^{α} dB(15)
			194	N_2H obB(14), N_2H obA(11)
		192		N_2H obB(16),CNC_2^{α} dB(14),N_2H obA(7)
201MW			191	N_2H obA(13),N_2H obB(8)
		190		CNC_2^{α} dA(12),N_2H obA(11)
			177	H··O s7(14),H··O s11(13)
		168		H··O s7(22),NC_2^{α}C dB(11),NC_1^{α}C dB(10), H··O s8(10)
		155		H··O s5(20),NC_2^{α}C dA(17),H··O s6(15), NC_3^{α}C dA(10)
			152	NC_2^{α}C dA(14),H··O s6(12),H··O s10(11), NC_3^{α}C dA(10),H··O s5(10)
			143	NC_3^{α}C dA(10),H··O s10(15),NC_2^{α}C dA(10)
		138		H··O s 10(23),H··O s11(15),NC_3^{α}C dA(10)
142M			138	NC_3^{α}C dB(19),NC_2^{α}C dB(13),CNC_2^{α} dB(10)
		136		H··O s11(21),NC_3^{α}C dB(16)
129VW		125		H··O s11(17),NC_3^{α}C dB(10)
			119	C_3^{α}C tB(23)
120MS		115		C_3^{α}C tB(32),N_3H obB(11),N_2H obB(9)
			115	H··O s11(23),H··O s5(10)
			103	H··O s1(15),H··O s6(10)
109W		101		H··O s6(21),NC_3^{α}C dA(13)
			91	H··O s11(21),H··O s10(14),C_3^{α}C tA(12),N_3H obA(9)

TABLE 3 (continued)

Observed[a]		Calculated		Potential energy distribution[b]
Raman	IR	g	u	
		89		H··O s1(27),N_3H obA(6)
90VW		88		$C_3^{\alpha}C$ tA(8)
			87	N_3H obA(14)
			80	H··O s2(26)
82VW		76		H··O s3(15)
			75	NC_3^{α} tB(20),$C_2^{\alpha}C$ tB(14),N_3H obB(7)
		73		NC_3^{α} tB(19),N_3H obB(6)
70VW		70		H··O s1(22), H··O s2(18)
65VW		63		NC_2^{α} tB(10)
			62	$C_1^{\alpha}C$ tB(25),H··O s5(16)
			60	NC_3^{α} tA(19)
		56		$C_1^{\alpha}C$ tB(24)
			53	H··O s2(9),H··O s4(9)
		53		NC_2^{α} tB(14),N_2H obB(11), C_2N tB(19)
50VW		51		CO··H b5(18),H··O s10(16),NC_3^{α} tA(10)
50W			50	$C_1^{\alpha}C$ tB(23)
		44		H··O s3(19),NH··O b3(19),N_2H obB(8)
			44	CO··H b5(10)
		41		H··O s8(9)
			37	H··O s10(16),H··O s5(12)
37sh		36		CO··H b4(14),NC_3^{α} tB(13),CO··H b1(10)
			34	H··O s4(12),N_2H obB(11)
		32		$C_2^{\alpha}C$ tA(13),$C_1^{\alpha}C$ tA(11)
			31	H··O s7(16),H··O s8(12),$C_2^{\alpha}C$ tA(11)
		30		H··O s8(11),H··O s10(11)
		26		H··O s2(7),N_2H obB(7)
			23	NH··O t4(10)
			23	$NC_2^{\alpha}C$ tB(13), N_2H obB(10)
		21		NH··O b2(15),CO··H b2(13),N_2H obA(6)
		17		CO··H tB(9), N_2H obB(9)
		15		C_2^{α} tB(18),NH··O b9(10),N_3H obB(7)
			12	NC_3^{α} tA(9),N_2H obB(7)
			9	CO··H b5(15),NC_2^{α} tA(11),N_2H obB(6)
		8		H··O s4(12),NH··O t1(12),CO··H b7(12)
				CO··H b8(12),CO··H b6(10)

[a]Bands marked with an asterisk are evident at low temperature.

[b]s, stretch; as, antisymmetric stretch; ss, symmetric stretch; b, bend; ib, in-plane bend; ob, out-of-plane bend; d, deformation; w, wag; tw, twist; r, rock; t, torsion. See Fig. 4. for designation of atoms, molecules and bonds. ($H_3=NH_3^+$, $O_2=CO_2^-$, $C_xH_2=C_x^{\alpha}H_2$.) Contributions $>10\%$ are shown except for NH modes for which contributions $>5\%$ are shown. Numbers in parentheses are calculated IR intensities. For differences in PEDs between g and u species of $<4\%$, average is given.

TABLE 4

Observed and calculated frequencies (in cm^{-1}) of N_1, N_2-Deuterated Gly_3

Observed[a]		Calculated		Potential energy distribution[b]
Raman	IR	g	u	
3312W	3313sh	3313	3313	N_3H sB(99)
3280MW	3280VS	3283	3284	N_3H sA(99)
	3095MW			Amide B
	3015W	3010	3010	C_3H_2 asB(100)
3008MW		3010	3010	C_3H_2 asA(100)
3000sh	2995W			
2976VW	2972VW			
2960VS		2957	2957	C_1H_2 asA(99)
		2956	2956	C_1H_2 asB(99)
2933S	2936M	2936	2936	C_3H_2 ssB(99)
		2936	2936	C_3H_2 ssA(99)
		2928	2928	C_2H_2 ssB(99)
		2927	2927	C_2H_2 asA(99)
2875VW		2881	2881	C_1H_2 ssB(99)
		2881	2881	C_1H_2 ssA(99)
	2855W	2861	2861	C_2H_2 ssB(99)
		2861	2861	C_2H_2 ssA(99)
2474W	2468MW			Amide B
2431W	2424S	2421	2421	N_2D sB(97)
	2408M	2417	2417	N_2D sA(97)
	2362W*	2355	2355	D_3 as1B(67),D_3 as2B(30)
		2350	2350	D_3 as1A(78),D_3 as2A(19)
	2345W*	2350	2350	D_3 as2B(67),D_3 as1B(30)
2331VW		2342	2342	D_3 as2A(79),D_3 as1A(19)
	2230VW	2207	2207	D_3 ssB(97)
	2180VW	2191	2191	D_3 ssA(98)
1687MW		1680		C_1O sB(73), C_1N sB(20),$C_1^{\alpha}CN$ dB(10)
	1674S		1677	C_1O sA(65),C_1N sA(17),$C_1^{\alpha}CN$ dB(10), [13.3]
		1674		C_1O sA(69),C_1N sA(18),$C_1^{\alpha}CN$ dA(10)
	1665sh*		1666	C_2O sA(65),C_2N sA(17),$C_2^{\alpha}CN$ dA(10) [6.0]
1658VS		1662		C_2O sB(72),C_2N sB(20),$C_2^{\alpha}CN$ dB(11)
			1655	C_1O sB(72),C_1N sB(20),$C_1^{\alpha}CN$ dB(10) [8.8]
1650sh		1652		C_2O sA(70),C_2N sA(18),$C_2^{\alpha}CN$ dA(10)
	1643VS		1646	C_2O sB(72),C_2N sB(20),$C_2^{\alpha}CN$ dB(11) [17.3]
1601W	1602VS	1581	1581	O_2 asB(104)
1583VW	1580sh	1576	1576	O_2 asA(104)
1557VW		1554		N_3H ibB(24),C_2N sB(14),$C_2^{\alpha}C$ sB(14),N_3H ibA(7)
	1554sh		1544	N_3H ibB(23),C_2N sB(14),$C_2^{\alpha}C$ sB(14),N_3H ibA(8) [8.4]
1529W		1537		N_3H ibA(22),$C_2^{\alpha}C$ sA(15),C_2N sA(13),N_3H ibB(8)
	1525W		1531	N_3H ibA(21),$C_2^{\alpha}C$ sA(14),C_2N sA(13),N_3H ibB(8) [0.6]
1484VW	1495sh	1500	1500	$C_1^{\alpha}C$ sA(31),C_1H_2 wA(20),C_1N sA(16), C_1H_2 bA(14),C_1O ibA(12), C_1O sA(10)

TABLE 4 (continued)

Observed[a]		Calculated		Potential energy distribution[b]
Raman	IR	g	u	
1475MW	1478MS	1496	1496	$C_1^{\alpha}C$ sB(29),C_1H_2 wB(17),C_1N sB(15), C_1H_2 bB(15),C_1O ibB(12),C_1O sB(12),N_2D ibB(5)
		1463	1463	C_3H_2 bA(27),C_2H_2 bA(15),O_2 ssA(15), C_3H_2 wA(11),C_2H_2 wA(10)
1459W	1458sh	1462	1462	C_2H_2 bB(31),C_3H_2 bB(20),O_2 ssB(10)
1442VS		1444	1444	C_2H_2 bB(27),C_3H_2 bB(27), C_1H_2 bB(21)
		1440	1441	C_2H_2 bA(36),C_3H_2 bA(19),C_1H_2 bA(19),N_3H bA(6)
	1432sh	1436	1436	C_1H_2 bB(56),C_2H_2 bB(19)
		1432	1432	C_1H_2 bA(63),C_2H_2 bA(14)
1429S	1426M	1414	1414	C_3H_2 bA(46),O_2 ssA(30),O_2 bA(12)
1421sh		1411	1411	C_3H_2 bB(44),C_3H_2 wB(19),O_2 ssB(18)
1406S		1405	1404	C_2H_2 bA(24),C_2H_2 wA(22),O_2 ssA(19), $C_3^{\alpha}C$ sA(14),C_3H_2 wA(14),N_3H ibA(8)
1386VW	1388W	1394	1394	O_2 ssB(32),C_2H_2 wB(23),$C_3^{\alpha}C$ sB(17), O_2 bB(14),N_3H ibB(10),C_2H_2 bB(10)
1376VW	1376S	1368	1368	C_3H_2 wA(33),C_2H_2 wA(29)
1365VW		1362	1362	C_1H_2 wB(29),C_3H_2 wB(23), C_2H_2 wB(20)
1352VW	1354sh	1355	1355	C_1H_2 wA(57),C_1N sA(14)
1337W	1337VW	1353	1353	C_1H_2 wB(39),C_2H_2 wB(15),C_3H_2 wB(13)
1316W				
1302MW	1305MS	1278	1278	C_2H_2 twA(86)
1281VW	1285sh*	1270	1270	C_1H_2 twB(64),C_2H_2 twB(24)
1272sh	1276W	1267	1267	C_1H_2 twA(80)
		1264	1264	C_3H_2 twB(35),C_2H_2 twB(26), N_3H ibB(6)
1260S	1261W	1260	1260	C_2H_2 twB(43),C_3H_2 twB(23),C_1H_2 twB(18)
1245W	1244W	1258	1258	C_3H_2 twA(67)
1238S		1227	1227	C_3H_2 twB(38), N_3H ibB(27), C_3H_2 wB(11)
1228W		1219	1219	N_3H ibA(33),C_3H_2 twA(28),C_3H_2 wA(14)
1188sh	1186sh	1174	1174	D_3 ab2A(56),D_3 ab1A(27),D_3 r1A(8)
1173W	1175MW	1162	1162	D_3 sbB(61),NC_1^{α} sB(36)
1158VW		1157	1157	D_3 ab1B(79)
		1152	1152	D_3 ab1A(63),D_3 ab2A(22),D_3 sbA(6)
		1151	1151	D_3 ab2B(85)
1148M	1144VW	1139	1139	D_3 sbA(70), NC_1^{α} sA(31), D_3 ab2A(12)
1132VW	1136sh*	1133	1133	NC_2^{α} sB(36), NC_1^{α} sB(20), D_3 sB(15)
1118MW	1113W	1103	1102	NC_1^{α} sA(44), NC_2^{α} sA(20), D_3 sbA(6)
1083W	1085W	1077	1077	NC_2^{α} sB(27),NC_1^{α} sB(23),C_1H_2 rB(12),D_3 sB(5)
1056VW	1060VW	1050	1050	NC_2^{α} sA(25),C_1H_2 rA(24),D_3 r2A(14),N_2D ibA(10)
1050sh		1041	1041	C_1H_2 rB(21),C_2H_2 rB(13),N_2D ibB(12),D_3 r2B(11)
1037MW	1037MS	1030	1030	C_1H_2 rB(27),N_2D ibB(15),D_3 r2B(13),C_2H_2 rB(10)
1031VW	1028sh*	1023	1024	N_2D ibA(25),$C_1^{\alpha}C$ sA(11)
1017VS	1019sh*	1018	1018	NC_2^{α} sA(21),C_1H_2 rA(20),NC_1^{α} sA(15),D_3 r2A(15)
991VS		1002	1002	NC_1^{α} sB(34),D_3 r1B(16),D_3 sbB(9)
	985MW	989	989	NC_1^{α} sA(29),D_3 r1A(16),D_3 sbA(7)

TABLE 4 (continued)

Observed[a]		Calculated		Potential energy distribution[b]
Raman	IR	g	u	
979sh		977	977	C_2H_2 rB(49),N_2D ibB(7)
972sh		976	976	$C_3^{\alpha}C$ sA(23),C_2H_2 rA(21)
		962	963	$C_3^{\alpha}C$ sB(32),O_2 bB(15)
951W		960	961	C_2H_2 rA(49)
			941	C_3H_2 rA(26),C_3H_2 rB(10),D_3 r1B(6)
939W		941		C_3H_2 rB(21),D_3 r1B(11)
933VW		941		C_3H_2 rA(39)
			941	C_3H_2 rA(18),C_3H_2 rB(17),D_3r1B(6)
923W		934	934	C_3H_2 rB(58),D_3 r1B(7)
915MW	918S	933	933	C_3H_2 rA(37),D_3 r1A(7)
900M	896sh*	905	907	N_2D ibB(27),$C_2^{\alpha}C$ sB(13), C_2N sB(10)
879S	881W	904	903	N_2D ibA(32)
846VW	845W	854	854	D_3 r1B(29),C_1N sB(3)
835VW	835VW	843	844	D_3 r1A(30),C_1N sA(10)
825VW		808	808	D_3 r2A(56),C_1H_2 rA(30)
788W	792W	803	803	D_3 r2B(59),C_1H_2 rB(26)
752VW	749W	746	746	O_2 bA(24),C_2N tA(16),O_2 ssA(10), N_3H obA(8)
738VW	734sh*	734	733	O_2 bB(27),O_2 ssB(11),$C_2^{\alpha}C$ sB(11),$C_3^{\alpha}C$ sB(11)
	725VS	711	711	C_2N tA(46),N_3H obA(18) [0.7]
		675	676	O_2 bA(17),$C_3^{\alpha}C$ sA(14), D_3 r1A(6)
		672	671	$C_3^{\alpha}C$ sB(13),C_2O ibB(12),O_2 bB(12),$C_1^{\alpha}C$ sB(12), D_3 r1B(7)
		638	637	C_1O obA(30),C_2O ibA(17)
		633	632	O_2 wB(31),C_1O obB(27),C_2O obB(12)
		629		O_2 wA(65),O_2 wB(19)
			629	O_2 wA(91)
		629		O_2 wB(38),O_2 wA(26)
	615sh*		629	O_2 wB(48),C_1O obB(13),N_3H obB(7)
	611M	614	613	C_2O obB(44),C_2N tB(20)
		609	608	C_1O obB(27),C_1O ibB(19),C_1^{α} sB(11)
606MW	607M*	606	607	C_2O obA(49),N_3 H obB(8),N_3H obA(6) [1.7]
587MW	586S	600	605	C_2N tB(54),N_3H obB(40) [0.6]
598MW		597		C_2O obA(21),C_1O obA(19),C_1O ibA(14),C_2N tB(13), N_3H obB(8)
583MW			586	C_2O obA(21),C_1O obA(20),C_1O ibA(14),C_2N tB(12),N_3H obB(7)
557W	544MS	572	573	O_2 rA(26),$C_2^{\alpha}CN$ dA(19)
524W	533MS	571	572	O_2 rB(24),$C_2^{\alpha}CN$ dB(20)
499sh	509W	501	501	C_1N tA(78),N_2D obA(43)
481M		455		$C_1^{\alpha}CN$ dA(18),O_2 rA(17)
	475S*		455	O_2 rB(27),$C_1^{\alpha}CN$ dB(24)
474M		454		O_2 rB(19),$C_1^{\alpha}CN$ dB(17)
	472S*		453	$C_1^{\alpha}CN$ dA(25),O_2 rA(24)
374MW		414	413	C_1N tB(120),N_2D obB(46)
321M		323	323	$C_2^{\alpha}CN$ dB(19),NC_1^{α} tB(12),$C_1^{\alpha}CN$ dB(10), O_2 rB(19)
302VW		317	318	$C_2^{\alpha}CN$ dA(21),O_2 rA(12),$C_1^{\alpha}CN$ dA(11),NC_1^{α} tA(10)

TABLE 4 (continued)

Observed[a]		Calculated		Potential energy distribution[b]
Raman	IR	g	u	
		297	297	N_3H obB(21),$C_3^{\alpha}C$ tB(18),N_2D obB(12)
		291	290	N_2D obA(16),$NC_1^{\alpha}C$ dA(15),$C_3^{\alpha}C$ tA(11),NC_1^{α} tA(10), N_3H obA(10)
287VW		285	284	NC_1^{α} tB(32),N_3H obB(8),N_2D obB(6)
		273	274	$C_3^{\alpha}C$ tA(18),$NC_1^{\alpha}C$ dA(12),N_3H obA(8),N_2D obA(5)
			268	C_2O ibB(14),CNC_3^{α} dB(12)
		265		$NC_1^{\alpha}C$ dB(16)
			263	$NC_1^{\alpha}C$ dB(15),N_2D obB(5)
259VW		261		C_2O ibB(16),CNC_3^{α} dB(15)
		257		CNC_3^{α} dA(13),C_2O ibA(11),N_3H obA(7)
			257	N_3H obA(13),CNC_3^{α}dA(12),$NC_3^{\alpha}C$ dA(11),C_2O ibA(10)
240VW		253	254	NC_1^{α} tA(22),$NC_1^{\alpha}C$ dB(12),N_3H obA(6)
		217	216	CNC_3^{α} dB(11),N_2D obB(5)
210VW		209	213	CNC_2^{α} dA(10),N_2D obB(5)
		182	183	N_2D obB(17),CNC_2^{α} dB(10),NC_1^{α} tB(10)
173VW		181	182	N_2D obA(18)
			172	H··O s7(14),$NC_1^{\alpha}C$ dB(11),H··O s11(10)
		163		H··O s7(20),$NC_2^{\alpha}C$ dB(13),$NC_1^{\alpha}C$ dB(11)
150VW		150		$NC_2^{\alpha}C$ dA(18),H··O s6(17),H··O s5(15),$NC_3^{\alpha}C$ dA(12)
			147	$NC_2^{\alpha}C$ dA(17),$NC_3^{\alpha}C$ dA(16),H··O s6(13)
			138	$NC_3^{\alpha}C$ dA(14),$NC_3^{\alpha}C$ dB(13)
		132		H··O s11(31),$NC_3^{\alpha}C$ dB(11)
		132		H··O s10(24)
			131	H··O s10(16),H··O s5(15)
126W		121		H··O s11(12),H··O s10(10)
			118	$C_3^{\alpha}C$ tB(24),N_3H obB(10),N_2D obB(5)
			112	H··O s11(27),H··O s5(15)
112VVW		111		$C_3^{\alpha}C$ tB(22),H··O s5(13),N_3H obB(8)
			101	H··O s1(15),H··O s6(11),N_2D obA(5)
98VVW		98		H··O s6(21),$NC_3^{\alpha}C$ dA(11),H··O s11(11)
		89		H··O s1(29),NC_3^{α} tA(10),N_3H obA(5)
89W		87		H··O s11(11),NC_2^{α} tA(10),$C_3^{\alpha}C$ tA(10),N_2D obA(6)
			87	H··O s11(22),H··O s10(18),$C_3^{\alpha}C$ tA(10),N_3H obA(6)
			85	N_3H obA(16)
			80	H··O s2(27)
77VVW		75		H··O s3(17)
			74	NC_3^{α} tB(14),$C_2^{\alpha}C$ tB(14),N_3H ob(7)
73VVW		73		NC_3^{α} tB(22),H··O s2(10),N_3H obB(6)
69VW		69		H··O s1(21),H··O s2(18)
61VW		62		NC_2^{α} tB(10)
			61	$C_1^{\alpha}C$ tB(25),H··O s5(16),NC_2^{α} tB(10)
			59	NC_3^{α} tA (19)

TABLE 4 (continued)

Observed[a]		Calculated		Potential energy distribution[b]
Raman	IR	g	u	
		55		$C_1^{\alpha}C$ tB(28)
53VW			52	H··O s4(10)
		52		NC_2^{α} tB(12),N_2D obB(8)
50VVW		51		CO··H b5(17),H··O s10(16),NC_3^{α} tA(10)
			49	$C_1^{\alpha}C$ tB(22)
			43	CO··H b5(10)
		43		NH··O b3(19),H··O s3(16),N_2D obB(7)
		40		NH··O b3(9)
37Wsh			37	H··O s10(16),H··O s5(13),H··O s11(10)
		36		CO··H b4(15),NC_3^{α} tB(12),CO··H b1(10)
			34	H··O s4(10),N_2D obB(10)
		32		$C_2^{\alpha}C$ tA(14),N_3H obA(5)
			30	H··O s7(16),H··O s8(12),$C_2^{\alpha}C$ tA(11)
		30		H··O s8(11),H··O s10(11),$C_1^{\alpha}C$ tA(10)
		25		$NC_2^{\alpha}C$ dB(8),N_2D obB(8)
			23	$C_2^{\alpha}C$ tB(13),NH··O t4(12)
			23	N_2D obB(11),$C_2^{\alpha}C$ tA(10),NC_2^{α} tB(10)
		21		NH··O b2(16),CO··H b2(13),N_2D obA(6)
		17		CO··H t3(10),N_2D obB(10)
		15		$C_2^{\alpha}C$ tB(19),NH··O b9(10),N_3H obB(7)
			12	$C_1^{\alpha}C$ tA(10),N_2D obB(8)
			9	CO··H b5(15),NC_2^{α} tA(11),CO··H b1(10)
		7		CO··H b7(14),CO··H b8(14),NH··O t1(10), H··O s4(13),CO··H b6(11),NH··O b1(10)

[a]Bands marked with an asterisk are evident at low temperature.[b]s, stretch; as, antisymmetric stretch; ss, symmetric stretch; b, bend; ib, in-plane bend; ob, out-of-plane bend; d, deformation; w, wag; tw, twist; r, rock; t,torsion. See Fig. 4 for designation of atoms, molecules and bonds. ($D_3=ND_3^+$, $O_2=CO_2^-$, $C_xH_2=C_x^{\alpha}H_2$.) Contributions > 10% are shown except for NH modes for which contributions > 5% are shown. Numbers in brackets are calculated IR intensities. For differences in PEDs between g and u species of < 4%, average is given.

The assignments of CH_2 s modes are reasonable, although we must leave open the possibility of some uncertainties because of Fermi resonances occurring as well in this region [24]. Nevertheless, the frequencies of the different CH_2 groups seem to segregate themselves and be reasonably well identified (our assignments for C_1H_2 follow those in diglycine [25], where bands are observed at 2960 and 2874 cm^{-1}, and similarly for C_3H_2 [25], where bands are observed at 3014 and 2926 cm^{-1}).

The amide I modes are quite well reproduced by the DDC calculation, in both frequencies and relative IR intensities, particularly when we consider that the unperturbed frequencies are predicted at about 1674, 1673, 1672, and 1662 cm^{-1} for both the A and B molecules (we do not have an explanation for the

IR doublet at 1685, 1680 cm^{-1}). The changes on deuteration are also reasonably well explained. The $N_1D_3^+ N_2HN_3D$ structure gives similar frequencies, so the amide I region does not provide a basis for distinguishing between the two kinds of deuterated molecules.

The NH_3^+ antisymmetric bend (ab) modes at 1630 and 1623 cm^{-1} are not well defined in the spectrum (in contrast to the case of Val-Gly-Gly [2], where they are observed at ~1610 cm^{-1}, MS, in the IR). Nevertheless, they are absent in the spectra of the deuterated Gly_3, and the appearance of the 1175 cm^{-1} ND_3^+ symmetric bend (sb) mode (in a clear region of the Gly_3 spectrum) again shows that this group was deuterated. The presence of weak bands near 1607R and ~1588R, IR cm^{-1} assignable to CO_2^- antisymmetric stretch (as) makes the assignment of the very strong band at 1602 cm^{-1} in deuterated Gly_3 to this mode seem strange, but a similar result was found in Val-Gly-Gly [2]: a very weak band at 1580 cm^{-1} (seen only at low temperature) was replaced on deuteration by a medium intensity band at 1589 cm^{-1}.

As can be seen from Table 3 there are no "pure" amide II modes, but NH in-plane bend (ib) is mixed with NH_3^+ sb. The unperturbed modes are calculated in the range 1547–1530 cm^{-1}, but DDC spreads these over the range 1574–1526 cm^{-1}. The frequency agreement with observed bands is quite good, and the strong IR bands at 1553 and 1538 cm^{-1} are well predicted by the intensity calculations (if not in the observed intensity ratio). The frequencies in the deuterated molecule are reasonably well predicted, although the relative intensities are not. This is probably a result of not having accurate enough eigenvectors at this, relatively unrefined, stage of the force field. In this case, the $N_1D_3^+ N_2HN_3D$ structure predicts a different pattern of amide II modes: 1562(g), 1551(g), 1546(u), and 1536(u) cm^{-1}; the observed pattern is in better agreement with the $N_1D_3^+ N_2DN_3H$ structure.

In the region of ~1470–1330 cm^{-1}, we find that there is significant mixing of CO_2^- symmetric stretch (ss) and CH_2 wag (w) with CH_2 b, so that it is difficult to speak of relatively pure modes. The calculations give a reasonable explanation of the observed bands of Gly_3. They also indicate that many of the modes change character on deuteration, which can account for the observed frequency as well as intensity changes. In particular, except for the observed bands at 1361 and 1416 cm^{-1}, the six frequency downshifts, the one essentially unchanged frequency (1415 cm^{-1}) and the one frequency upshift (1349 cm^{-1}) predicted on deuteration are seen in the behavior of the observed bands.

In the ~1300–1220 cm^{-1} region, we find CH_2 twist (tw) mixed differentially with NH ib: CH_2 tw dominates above 1260 cm^{-1} while NH ib predominates below. As a result, deuteration has a non-trivial effect above 1260 cm^{-1} (cf. the significant changes in calculated modes at 1284, 1276 and 1261 cm^{-1}, and the associated changes in observed frequencies and intensities) in addition to the changes seen below 1260 cm^{-1} associated with N_2H to N_2D conversion. In the latter case it is important to note that, while the N_2H ib component of the

1244 cm^{-1} Raman band probably contributes to its significant intensity in Gly_3, this band does not disappear on deuteration since the CH_2 twist contribution to the original mode is expected to persist (and be enhanced) at about the same frequency in the deuterated molecule. In the $N_1D_3^+ N_2HN_3D$ structure the predominant N_2H ib modes are predicted at 1243 and 1234 cm^{-1}, which are in better agreement with the observed bands than that given by the $N_1D_3^+ N_2DN_3H$ structure.

The NH_3^+ rock (r) modes are predicted in the 1210–1150 cm^{-1} region, and seem to be well assigned to observed bands. As expected, these disappear on deuteration, but are replaced in this region by ND_3^+ ab and sb modes. Thus, the apparent shift of the 1153 cm^{-1} Raman band to 1148 cm^{-1} in the deuterated molecule is in fact a replacement of an NH_3^+ r mode by an ND_3^+ sb mode.

The NC^α s modes are expected to contribute in the 1100 to $\sim$1000 cm^{-1} region, and the match between observed and calculated frequencies is quite good. The strong Raman band observed at 1000 cm^{-1} is predicted to shift up by 17 cm^{-1} on deuteration, probably as a result of the admixture of ND_3^+ r, and such a shift is indeed observed. Other NC^α s modes are predicted to mix with ND_3^+ r to shift down, to 1002 and 989 cm^{-1}, and a very strong band at 991 cm^{-1} in the Raman and a new band at 985 cm^{-1} in the IR are assignable to these modes. It might seem that from its position, the medium intensity Raman band at 992 cm^{-1} should be assigned to a skeletal rather than to a C_2H_2 r mode. However, we are inclined to accept the present assignment by analogy with the situation in Val-Gly-Gly [2], where C_2H_2 r modes are also predicted at 994 and near 965 cm^{-1}, namely 972 cm^{-1}, although the strong Raman band is observed near the lower frequency, namely at 965 cm^{-1}. For the $N_1D_3^+ N_2HN_3D$ structure, the agreement in this frequency region is generally poorer, with particularly bad agreement for N_3D modes, calculated at 1018 and 1017 cm^{-1}, compared to 1030 and 1024 cm^{-1} in the present case.

The region down to $\sim$720 cm^{-1} contains CH_2r modes, in some cases combined with NH_3^+ r, and CO_2^- b modes. The small observed downward shifts of the latter on deuteration are well predicted. So is the upward shift of the 909 cm^{-1} Raman band to 915 cm^{-1}, with the appearance of a new strong 918 cm^{-1} IR band, probably mainly as a result of the replacement of NH_3^+ r by ND_3^+ r. New bands at 900 and 879 cm^{-1} in the Raman are well assigned to N_2D ib, and the four new bands in the $\sim$850–790 cm^{-1} region correspond reasonably to expected ND_3^+ r modes.

The amide V mode is composed mainly of CN torsion (t) and NH out-of-plane bend (ob), and its frequency is particularly sensitive to the strength of the hydrogen bond [1]. In Gly_3NH ob is associated with bands calculated at 720, 690, 680, 643, 609, and 563 cm^{-1}, and assignable bands of appropriate IR intensity are observed at 718, 706, 695, 648, 607, and 555 cm^{-1}, respectively. The frequency and intensity agreement, while not good for some bands, is acceptable at this stage in view of the lack of refinement of f(NH ob) and f(NH ob, CN t). Upon deuteration, most of the observed bands disappear or shift,

and the new frequencies are reasonably well predicted by the calculation. A comparison with calculated values for $N_1D_3^+ N_2HN_3D$ also favors the $N_1D_3^+ N_2DN_3H$ structure. The 720 cm^{-1} mode is predicted to decrease to 711 cm^{-1}; in fact, it is observed to increase from 718 to 725 cm^{-1} and to intensify (although more than computed). However, for $N_1D_3^+ N_2HN_3D$ no band is predicted in this region. The N_2H obA modes observed at 706 and 695 cm^{-1} disappear, as expected, on deuteration, with N_2D obA being predicted at 501 and a new band observed at 509 cm^{-1}; for the alternate deuteration possibility N_2H obA is predicted to contribute to strong bands at 687 and 673 cm^{-1}, where no IR bands are observed. The N_3H obB mode calculated at 609 cm^{-1}, with a suitably strong band being observed at 607 cm^{-1}, is predicted to split into two modes at 607 and 605 cm^{-1}; two bands are assignable to these new modes, at 607 and 586 cm^{-1}, although their relative intensity is reversed. For $N_1D_3^+ N_2HN_3D$, a small contribution of N_3D obB is predicted at 610 cm^{-1} (the main contribution being CO ob), with the next lower ob mode being N_2H obB at 555 cm^{-1}. Finally, the N_2H obB mode calculated at 563 and observed at 555 cm^{-1} is predicted to shift down to 414 cm^{-1}, to which the 374 cm^{-1} Raman band may be assignable. For $N_1D_3^+ N_2HN_3D$, N_3D obA is predicted at 520 cm^{-1}, with the only other such mode over 300 cm^{-1} being N_3D obB at 441 cm^{-1}.

Several conclusions emerge from these results. First, an NH group still remains on deuteration: there can be no other explanation for the strong 725 cm^{-1} band. Second, although this part of the force field needs further refinement, the spectral data strongly favor $N_1D_3^+ N_2DN_3H$ over $N_1D_3^+ N_2HN_3D$ for this species; this is in agreement with deductions from the NH s region. Third, a major puzzle remains: the CO_2^- modes calculated at 581 and 580 cm^{-1}, and satisfactorily assigned to bands at $\sim$580 and 573 cm^{-1}, respectively, are predicted to shift down to 573 and 572 cm^{-1} on deuteration; the bands appear to shift by much more, to 544 and 533 cm^{-1}. If this assignment is correct, it may indicate that some force constants associated with the CO_2^- group need further refinement, or that the structure changes slightly on deuteration (which might also explain some of the large discrepancies in NH ob modes).

For bands below 400 cm^{-1}, reasonable assignments can be made for both the protonated and deuterated molecules, though these will clearly need additional confirmation. As might be expected, in this region there are no significant differences predicted between the $N_1D_3^+ N_2DN_3H$ and $N_1D_3^+ N_2HN_3D$ structures. It is noteworthy, however, that frequency shifts in this region are also consistent with the existence of a partially deuterated molecule.

CONCLUSIONS

We have done normal coordinate analyses of the unit cell structures of crystalline Gly_3 [4], containing an asymmetric unit of two molecules, and of a

partially deuterated derivative corresponding to (as indicated by a comparison of analyses of the different possible structures) $N_1D_3^+ N_2DN_3H$. We used our polyglycine I force field [13] for these calculations.

For the protonated molecule, the agreement between observed and calculated frequencies, as well as IR intensities for some of the amide modes, is quite good: the average discrepancy for 80 convincingly assignable observed frequencies between 1800 and 200 cm^{-1} is 6.3 cm^{-1}, with there being two above 20 cm^{-1}, five above 15 cm^{-1}, and seventeen above 10 cm^{-1}. For the deuterated molecule, as expected, the average discrepancy in this range is larger, being 8.7 cm^{-1}. Since the force field was transferred without complete refinement, we believe that these results are quite satisfactory.

When we consider the above results in the context of the complexity of the structure of Gly_3, it is evident that the present force fields [1] are substantively capable of reproducing in significant detail the normal modes of peptide molecules. This shows that such analyses can provide a rigorous base for the IR and Raman study of the conformations of peptides and proteins.

ACKNOWLEDGEMENTS

This research was supported by NSF grants DMB-8816756 and DMR-8806975. One of us (T. S.) wishes to acknowledge support from the Macromolecular Research Center of The University of Michigan, an ASLA-Fulbright Research Grant, and the Finnish Society of Sciences and Letters. We are indebted to Dr. R. Parthasarathy for X-ray analyses of our crystals.

REFERENCES

1 S. Krimm and J. Bandekar, Adv. Protein Chem., 38 (1986) 181.
2 J. Bandekar and S. Krimm, Biopolymers, 27 (1988) 885.
3 J. Bandekar and S. Krimm, Biopolymers, 27 (1988) 909.
4 T. Srikrishnan, N. Winiewicz and R. Parthasarathy, Int. J. Peptide Protein Res., 19 (1982) 103.
5 J.D. Bernal, Z. Kristallogr., 78 (1931) 363.
6 F.V. Lenel, Z. Kristallogr., 81 (1932) 224.
7 E.W. Hughes and W.J. Moore, Acta Crystallogr., 3 (1950) 313.
8 H.I. Yakel and E.W. Hughes, Acta Crystallogr., 5 (1952) 847.
9 A. Theorét, Y. Grenié and C. Garrigou-Lagrange, J. Chim. Phys. Physiochim. Biol., 66 (1969) 1196.
10 M. Smith, A.G. Walton and J.L. Koenig, Biopolymers, 8 (1969) 29.
11 H.S. Randhawa and C.N.R. Rao, J. Cryst. Mol. Struct., 3 (1973) 309.
12 C. Destrade and C. Garrigou-Lagrange, J. Mol. Struct., 31 (1976) 301.
13 A.M. Dwivedi and S. Krimm, Macromolecules, 15 (1982) 177.
14 T. Sundius and S. Krimm, Proc. IXth Int. Conf. Raman Spectroscopy, Tokyo, Japan, 1984, p. 602.
15 R. Parthasarathy, private communication.

16 B. Lotz, J. Mol.Biol., 87 (1974) 169.
17 H.C. Freeman, G.L. Paul and T.M. Sabine, Acta Crystallogr., Sect. B, 26 (1969) 925.
18 A. Kvick, A.R. Al-Karaghouli and T.F. Koetzle, Acta Crystallogr., Sect. B, 33 (1977) 3796.
19 T.C. Cheam and S. Krimm, J. Mol. Struct., 146 (1986) 175.
20 T.C. Cheam and S. Krimm, J. Mol. Struct., (1988), 193 (1989) 1.
21 C. Destrade, E. Dupart, M. Joussot-Dubien and C. Garrigou-Lagrange, Can. J. Chem., 52 (1974) 2590.
22 T.C. Cheam and S. Krimm, J. Chem. Phys., 82 (1985) 1631.
23 S. Krimm and A.M. Dwivedi, J. Raman Spectrosc., 12 (1982) 133.
24 R.G. Snyder, S.L. Hsu and S. Krimm, Spectrochim. Acta, Part A, 34 (1978) 395.
25 P. Lagant, G. Vergoten, M.H. Loucheaux-Lefebvre and G. Fleury, Biopolymers, 22 (1983) 1267.